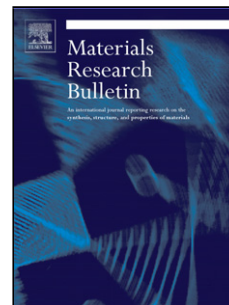


Accepted Manuscript

Title: $\text{Ag}_2\text{O}/\text{Ag}_3\text{VO}_4/\text{Ag}_4\text{V}_2\text{O}_7$ heterogeneous photocatalyst prepared by a facile hydrothermal synthesis with enhanced photocatalytic performance under visible light irradiation

Author: Rong Ran Joanne Gamage McEvoy Zisheng Zhang



PII: S0025-5408(15)30094-5
DOI: <http://dx.doi.org/doi:10.1016/j.materresbull.2015.08.028>
Reference: MRB 8381

To appear in: *MRB*

Received date: 13-5-2015
Revised date: 11-8-2015
Accepted date: 22-8-2015

Please cite this article as: Rong Ran, Joanne Gamage McEvoy, Zisheng Zhang, $\text{Ag}_2\text{O}/\text{Ag}_3\text{VO}_4/\text{Ag}_4\text{V}_2\text{O}_7$ heterogeneous photocatalyst prepared by a facile hydrothermal synthesis with enhanced photocatalytic performance under visible light irradiation, Materials Research Bulletin <http://dx.doi.org/10.1016/j.materresbull.2015.08.028>

This is a PDF file of an unedited manuscript that has been accepted for publication. As a service to our customers we are providing this early version of the manuscript. The manuscript will undergo copyediting, typesetting, and review of the resulting proof before it is published in its final form. Please note that during the production process errors may be discovered which could affect the content, and all legal disclaimers that apply to the journal pertain.

Ag₂O/Ag₃VO₄/Ag₄V₂O₇ heterogeneous photocatalyst prepared by a facile hydrothermal synthesis with enhanced photocatalytic performance under visible light irradiation

Rong Ran^{a,b}, Joanne Gamage McEvoy^{a,b}, Zisheng Zhang^{a,b,*}

^a Department of Chemical and Biological Engineering, University of Ottawa, Ottawa, Ontario, K1N 6N5, Canada

^b Centre for Catalysis Research and Innovation, University of Ottawa, Ottawa, Ontario, K1N 6N5, Canada

*Corresponding author. Tel.: +1 613 562 5800 x 6110; fax: +1 613 562 5172; Email: zzhang@uottawa.ca

Graphical abstract

Highlights

- The photocatalyst was hydrothermally prepared by adjusting the ratio of Ag to V.
- Multi-phase Ag₂O/Ag₃VO₄/Ag₄V₂O₇ obtained exhibited multi-morphological features.
- The photocatalyst exhibited strong visible light driven photoactivity towards RhB.

Abstract

A novel $\text{Ag}_2\text{O}/\text{Ag}_3\text{VO}_4/\text{Ag}_4\text{V}_2\text{O}_7$ photocatalyst was synthesized by adjusting the molar ratio of silver to vanadium (Ag to V) in a facile hydrothermal method to obtain multi-phase $\text{Ag}_2\text{O}/\text{Ag}_3\text{VO}_4/\text{Ag}_4\text{V}_2\text{O}_7$ photocatalyst. The photocatalytic activity of the prepared samples was quantified by the degradation of Rhodamine B (RhB) model organic pollutant under visible light irradiation. Compared to pure Ag_3VO_4 , $\text{Ag}_4\text{V}_2\text{O}_7$ and P25 TiO_2 , respectively, the as-synthesized multi-phase $\text{Ag}_2\text{O}/\text{Ag}_3\text{VO}_4/\text{Ag}_4\text{V}_2\text{O}_7$ powders gave rise to a significantly higher photocatalytic activity, achieving up to 99% degradation of RhB in 2 h under visible light. This enhanced photocatalytic performance was attributed to the effect of the multi-phase $\text{Ag}_2\text{O}/\text{Ag}_3\text{VO}_4/\text{Ag}_4\text{V}_2\text{O}_7$ photocatalyst and the surface plasmon resonance (SPR) of the incorporated metallic silver (Ag^0) nanoparticles (NPs) generated during the photocatalysis, as evidenced by post-use characterization, resulting in improved visible light absorption and electron-hole (e^-h^+) separation. A mechanism was proposed for the photocatalytic degradation of RhB on the surface of $\text{Ag}_2\text{O}/\text{Ag}_3\text{VO}_4/\text{Ag}_4\text{V}_2\text{O}_7$.

Keywords: Semiconductors; Solvothermal; Chemical synthesis; Catalytic properties; Optical properties

1. Introduction

Strategies for the development of ternary metal oxides have been investigated in recent years as an alternate route for the fabrication of highly efficient photocatalysts, which can be used for photocatalytic degradation and water splitting applications [1-4]. Numerous ternary metal oxide photocatalysts have been reported in literature, such as Ag_3VO_4 [5], $\text{Ag}_4\text{V}_2\text{O}_7$ [6], $\beta\text{-AgVO}_3$ [7], AgNbO_3 [8], AgMO_2 ($M = \text{Al, Ga, In}$) [9, 10], Ag_2CO_3 [11], and Ag_3PO_4 [12] and have been found to exhibit enhanced photocatalytic performance under visible light irradiation (VLI), compared to the traditional TiO_2 photocatalyst [13].

Despite these research efforts, single phase ternary metal oxide photocatalysts tend to suffer from poor visible light absorption due to the number of grain boundaries present [1, 14]. These defects usually serve as recombination centers, and impede the effective transfer of the photogenerated electrons (e^-) and holes (h^+) to adsorbed organic pollutants by trapping the separated charge species [1, 14, 15]. In addition, large specific surface area is a prerequisite for the effective photocatalytic degradation of organic pollutants, as it contributes to increasing the transfer rate of photogenerated charges, improving carrier separation, and increasing surface reactivity during adsorption-desorption equilibration [16-20].

An approach to improving photocatalytic performance under VLI has been in the development and preparation of heterogeneous photocatalysts based upon silver species. For example, Xue et al [21] reported that novel $\text{Ag}_2\text{O}/\text{N}$ -doped helical carbon nanotubes ($\text{Ag}_2\text{O}/\text{N}$ -HCNTs) were successfully synthesized via a simple co-precipitation of N-HCNTs and Ag_2O , respectively, which gave rise to the high photocatalytic performance towards degradation of methylene blue (MB) and showed good stability in multiple degradation cycles under visible light irradiation. Similarly, Wang et al. [22] investigated $\text{Ag}_2\text{O}/\text{Ag}_3\text{PO}_4$ heterostructured photocatalyst prepared by ion-exchange synthesis of Ag_3PO_4 and subsequent precipitation. The heterostructures prepared exhibited a much higher degradation of methyl orange (MO) and phenol than the pure Ag_3PO_4 , and possessed good stability in the aqueous photosystem under VLI. Highly efficient p-n junction Ag_2O -decorated flower-like ZnO photocatalyst exhibited high photoactivity towards MO under ultraviolet (UV) irradiation by transferring photogenerated carriers and suppressing the e-h recombination rate [23]. Zhou et al. [24] reported that the photocatalytic activity of $\text{Ag}_2\text{O}/\text{TiO}_2$ nanobelts' heterostructure was attributed to the Ag_2O NPs scattered uniformly on the surface of TiO_2 , giving rise to the higher photocatalytic decomposition of MO under both UV and VLI. However, the conventional syntheses employed to prepare these heterostructure-containing visible-light-induced photocatalysts are multi-step, time-consuming

procedures. Therefore, in this work, we propose a facile approach to obtain multi-phase $\text{Ag}_2\text{O}/\text{Ag}_3\text{VO}_4/\text{Ag}_4\text{V}_2\text{O}_7$ photocatalyst with high photocatalytic performance under VLI, fabricated via a hydrothermal process and changing the ratio of elements employed in the synthesis procedure. The prepared photocatalysts were then studied for the degradation of RhB organic dye. The novel heterogeneous $\text{Ag}_2\text{O}/\text{Ag}_3\text{VO}_4/\text{Ag}_4\text{V}_2\text{O}_7$ photocatalyst could improve the utilization of light to enhance the degradation of organic pollutants via the synergistic effects among these three photosensitive phases. To the best of our knowledge, this approach to the preparation of multi-phase $\text{Ag}_2\text{O}/\text{Ag}_3\text{VO}_4/\text{Ag}_4\text{V}_2\text{O}_7$ has not yet been reported.

2. Experimental

2.1. Synthesis

Multi-phase $\text{Ag}_2\text{O}/\text{Ag}_3\text{VO}_4/\text{Ag}_4\text{V}_2\text{O}_7$ photocatalyst was synthesized via hydrothermal method using potassium metavanadate (KVO_3) and silver nitrate as starting materials. KVO_3 was prepared by calcination, where 0.38 g K_2CO_3 (Fisher Scientific, Certified ACS) and 0.5 g V_2O_5 (ACROS Organics, 99.6%) were dissolved in 35 mL deionized water (DW) under vigorous magnetic stirring. The resulting red solution was poured into an evaporation dish, and dried overnight at 50 °C in an oven (Sheldon Manufacturing, Inc. Model No: 1350 GM). The dry sample was then ground in an agate mortar and annealed in air at 457 °C (730 K)

for 5 h, yielding a pink KVO_3 powder. To prepare the multi-phase $\text{Ag}_2\text{O}/\text{Ag}_3\text{VO}_4/\text{Ag}_4\text{V}_2\text{O}_7$ powders, the molar ratio of silver to vanadium (Ag to V) used was 6:1.5. 15 mL of as-prepared KVO_3 solution was heated in a water bath at 60 °C for 3 min, and 60 mL of 0.1 M AgNO_3 (Fisher Scientific, Certified ACS) was then added dropwise and allowed to react under continuous stirring for 30 min to obtain an orange-yellow slurry. The pH of the resulting slurry was then adjusted by adding 1M KOH , until a final pH of 7 was reached, as measured by a pH meter (Fisher Scientific, accumet basic, AB 15 pH meter). The slurry was then transferred into 45 mL Teflon-lined stainless steel autoclave reactors, and the reaction was allowed to proceed at 140 °C for 8 h. The resulting solid was collected by filtration, washed five times with DW, and dried in an oven at 110 °C for 6 h. The temperatures and times selected for the hydrothermal process were based upon the study by Huang et al. [25].

For comparison, pure Ag_3VO_4 was also prepared via the described method, but applying a molar ratio of Ag to V of 3: 1. Single phase $\text{Ag}_4\text{V}_2\text{O}_7$ (Ag to V of 3: 1) was also similarly prepared, but adding Cetyltrimethyl Ammonium Bromide (CTAB, $\text{C}_{19}\text{H}_{49}\text{BrN}$) (ACROS Chemical, 99 + %) as a structural agent at a molar ratio of 0.05:1 (CTAB: silver), in accordance with the report of Huang et al. [25, 26].

2.2. Characterization

Powder X-ray diffraction (XRD) measurements were carried out in Bragg–Brentano geometry on a Rigaku Ultima IV apparatus with Cu K α 1 ($\lambda = 0.15418$ nm) radiation, operating at 40 kV and 44 mA, and with a scanning range of 2θ from 15° to 70° . Transmission electron microscopy (TEM) images were obtained using an FEI (formerly Phillips) Tecnai G2 F20 field emission transmission electron microscope at an acceleration voltage of 200 keV. Scanning electron microscopy (SEM) images were obtained with a Tescan VegaII XMU electron microscope operated at 20 kV, with Au/Pd alloy coated samples (coated with an Anatech Hummer VII sputter coater). SEM-EDS was performed using an energy dispersive X-ray detector. X-ray photoelectron spectroscopy (XPS) was conducted on a Kratos Analytical Axis Ultra DLD instrument with mono-chromated Al X-rays at 140 W. The powder UV-Vis diffuse reflectance spectra (DRS) were recorded on a Thermo Evolution 300 UV/Vis spectrophotometer equipped with a Praying Mantis diffuse reflectance accessory, and the spectra were collected at a scan rate of 240 nm min^{-1} . UV/Vis spectra of RhB samples were obtained via a Biochrom Ultrospec 60 UV/Vis spectrophotometer.

2.3. Photocatalytic activity

Photocatalytic performance was quantified by the decomposition of RhB (Sigma-Aldrich) as a model organic pollutant under VLI. A slurry reactor was placed in a reflective housing to prevent outside light from entering the reactor, and inside light from exiting the system. A 300 W ELH tungsten halide bulb (Ushio) was used as a light source with a 410 nm cut-off filter (Kenko Zeta, $\lambda > 410$ nm, transmittance $> 90\%$) to provide visible light irradiation. The light source was placed at a distance of 15 cm from the top of the slurry. The corresponding irradiation was measured using a quantum meter (Biospherical QSL-2100; 400 nm $< \lambda < 700$ nm), and was found to be approximately 10.9×10^{-3} Einstein $\text{m}^{-2} \text{s}^{-1}$. Cooling was provided by an external cooling jacket, and the temperature of the reaction was controlled to $20 \text{ }^\circ\text{C} \pm 2$. Before illumination, 0.15 g of photocatalyst dispersed into 150 mL of 15 mg L^{-1} RhB solution was allowed to reach adsorption-desorption equilibrium under continuous magnetic stirring at 280 rpm for 30 min in the dark. Irradiation was then provided for 2 h. Samples were withdrawn at 15 min time intervals and separated by centrifugation at 10×10^3 rpm for 3 min in an accuSpin Micro 17 (Fisher Scientific) microcentrifuge to remove the suspended catalyst. The supernatant fluid was then analyzed by monitoring the peak absorbance ($\lambda = 554$ nm for RhB) with a Genysys 10-UV spectrophotometer (Geneq Inc.). A standard curve for RhB was prepared and the concentration was

determined by the measured absorbance and the Beer-Lambert Law. In the recyclability studies, the used, unwashed photocatalysts were separated by centrifugation after each run, the degraded RhB supernatant removed, and fresh 15 mg L⁻¹ RhB solution added. The roles of various reactive species were studied by employing reactive species scavengers (including tert-butyl alcohol (TBA) (Sigma-Aldrich, ACS), benzoquinone (BQ) (reagent-grade \geq 98%, Sigma Aldrich) and ammonium oxalate (AO) (ACS, Sigma-Aldrich)), using the same procedures and methodology described above.

3. Results and discussion

3.1. XRD analysis

The XRD pattern of the fresh, multi-phase photocatalyst obtained via hydrothermal synthesis is shown in Fig. 1. The pattern observed was found to exhibit features of the α -Ag₃VO₄ (JCPDS Card No. 01-077-5276), Ag₄V₂O₇ (JCPDS Card No.01-077-0097), and silver oxide phases (JCPDS Card No. 00-041-1104), respectively. The major reflections for the α -Ag₃VO₄ phase occurred at 32.42° (3 1 2) and 30.96° (1 1 2), while the major peaks of the Ag₄V₂O₇ structure were observed at 32.93° (0 4 0) and 31.93° (2 2 4), and the reflection of the silver oxide peaks was identified at 32.79° (1 1 1) and 38.07° (2 0 0) with low intensity, suggesting that a low amount of Ag₂O was present in the fresh sample.

3.2. TEM analysis

As shown in Fig. 2a and 2b, the fresh multi-phase $\text{Ag}_2\text{O}/\text{Ag}_3\text{VO}_4/\text{Ag}_4\text{V}_2\text{O}_7$ photocatalyst was observed to range from 0.5 μm to 4 μm , and was decorated with Ag_2O NPs clusters ranging from 50 nm to 180 nm; similar results were reported by Yang et al. [27].

As seen in Fig. 2c, the high-resolution TEM (HRTEM) of the multi-phase $\text{Ag}_2\text{O}/\text{Ag}_3\text{VO}_4/\text{Ag}_4\text{V}_2\text{O}_7$ photocatalyst exhibited lattice spacings of 0.27 nm and 0.24 nm, which corresponded to *d-spacings* of Ag_2O (1 1 1) and (2 0 0) planes of silver oxide. Also, the selected area electron diffraction (SAED) patterns shown in the inset of Fig. 2c further confirmed the crystal structure of Ag_2O present in the multi-phase crystalline structure of $\text{Ag}_2\text{O}/\text{Ag}_3\text{VO}_4/\text{Ag}_4\text{V}_2\text{O}_7$ photocatalyst, demonstrating that the as-prepared silver species sample was polycrystalline structure in nature. The rings were ascribed to diffraction from the (1 1 1) and (2 0 0) reflections of Ag_2O phase (JCPDS Card No. 00-041-1104), based on the calculated *d-spacings* of 2.73 Å and 2.36 Å, respectively.

3.3. SEM and EDS analyses

The morphologies present in the synthesized multi-phase $\text{Ag}_2\text{O}/\text{Ag}_3\text{VO}_4/\text{Ag}_4\text{V}_2\text{O}_7$ photocatalyst were explored by SEM. The corresponding EDS spectra were also studied to qualitatively investigate the components present

in the $\text{Ag}_2\text{O}/\text{Ag}_3\text{VO}_4/\text{Ag}_4\text{V}_2\text{O}_7$ photocatalyst, and the results are shown in Figs. 3a and 3b, respectively.

As shown in Fig. 3a, the fresh $\text{Ag}_2\text{O}/\text{Ag}_3\text{VO}_4/\text{Ag}_4\text{V}_2\text{O}_7$ photocatalyst exhibited plate-like morphology with size ranges from 0.5 μm to 4 μm , which agreed with the results reported by Pan et al. [28], and were sparsely decorated with Ag_2O NPs, agreed with the report by Zhou et al. [24] and the results observed from XRD and TEM. According to the results shown in Fig. 3b, EDS data showed that only the silver, vanadium and oxygen elements constituted the as-synthesized sample. The results indicated that no other elements occurred as impurities in the prepared $\text{Ag}_2\text{O}/\text{Ag}_3\text{VO}_4/\text{Ag}_4\text{V}_2\text{O}_7$. It should be noted that the Au peak occurred as a result of the sputter coating, and carbon was attributed to the adsorbed carbon present in the samples.

3.4. XPS analysis

To investigate the chemical and electronic states present in the prepared multi-phase photocatalyst, XPS analyses of the fresh $\text{Ag}_2\text{O}/\text{Ag}_3\text{VO}_4/\text{Ag}_4\text{V}_2\text{O}_7$ were conducted, and the corresponding high resolution XPS spectral patterns are shown in Figs. 4a, 4b and 4c, for Ag 3d, V 2p and O 1s states, respectively.

As shown in Fig. 4a, the spectra of the Ag species exhibited two symmetric peaks located at binding energies of 367.5 eV and of 373.5 eV, with a separation of

6 eV, ascribed to the spin-orbit splitting characteristic of Ag 3d_{5/2} and Ag 3d_{3/2}, respectively, and corresponding to Ag⁺ [29, 30]. The binding energy observed at 367.5 eV and 373.5 eV indicated that silver was probably in the state of oxides [31], agreeing with the results in shown in XRD and SEM. No peaks attributable to Ag⁰ (located at 368.3 eV and 374.5 eV) [30, 32, 33] were observed, indicating that no Ag⁰ NPs existed in the fresh sample.

The observed peak shown in Fig. 4b at a binding energy of 516.4 eV was attributed to the V 2p_{3/2} orbital, and that at 523.8 eV to the V 2p_{1/2} orbital, indicating that the vanadium was present in the form of V⁵⁺ [7], which corresponds well with the data expected from KVO₃ [34].

The oxygen peak in Fig. 4c for the O 1s spectra was observed to be broad and was deconvoluted into three separate peaks (dashed lines in Fig. 4c). The main peak occurring at binding energy of 530.9 eV was thought to be dominant, while the peaks located at binding energies of 532.1 eV and 534.5 eV were of lower intensity, and indicated that the oxygen species was not purely ionic but also contained metal-oxygen bonds with covalent characteristics [29]. The main peak at 530.9 eV was considered to be oxygen species in the presence of covalent mixing states. As reported in literature, the oxide ions, such as O²⁻, would have given rise to a single Gaussian peak around 532 eV [29]. However, the results obtained indicated that the oxygen species present contained mainly covalent characteristics

in the presence of dominant metal-oxygen bonds rather than pure oxide ionic states. This covalent characteristic with metal-oxygen bonds promoted a shift of the broad oxygen peak observed, in which binding energies of 532.1 eV and 534.5 eV were attributed to the lattice oxygen in the multi-phase silver speices composite, and the absorbed oxygen, respectively [35]. Therefore, the results suggested the existence of covalent bonding including the Ag-O bonding [36] and between the vanadium and oxygen in the form of $(VO_4)^{3-}$ and $(V_2O_7)^{4-}$ species [29], respectively, which were also confirmed with the results in SAED patterns and EDS data present in the previous section.

3.5. Optical properties

In order to estimate the band gap energy of the fresh $Ag_2O/Ag_3VO_4/Ag_4V_2O_7$, UV-Vis diffuse reflectance spectra of the samples were investigated and the corresponding patterns indicating intrinsic absorption in the visible light region are shown in Fig. 5.

The band gap energies of the as-prepared fresh catalysts were estimated by the DRS data and the following equation:

$$\lambda = 1240/E_{bg}. \quad (1)$$

Where λ is the maximum wavelength of absorption by photocatalysts (nm) (illustrated by the tangent lines in Fig. 5), and E_{bg} is the estimated band gap energy of the photocatalysts (eV).

As shown in Fig. 5, the onset of visible light absorption by $\text{Ag}_2\text{O}/\text{Ag}_3\text{VO}_4/\text{Ag}_4\text{V}_2\text{O}_7$ occurred around 625 nm, resulting in a calculated band gap energy of ~ 1.98 eV, which was smaller than that of both Ag_3VO_4 ($E_{bg} = 2.1$ eV) and $\text{Ag}_4\text{V}_2\text{O}_7$ ($E_{bg} = 2.5$ eV), agreeing with the results from literature [6, 25, 37]. This improved visible light absorption observed in the multi-phase photocatalyst was thought to be due to the presence of Ag_2O ($E_{bg} = 1.29$ eV) [38], where more visible light could be absorbed by these incorporated species containing narrower band gap energy.

3.6. Photocatalytic activity of $\text{Ag}_2\text{O}/\text{Ag}_3\text{VO}_4/\text{Ag}_4\text{V}_2\text{O}_7$

3.6.1. Photodegradation of RhB

To quantify photocatalytic activity, RhB was used as a model organic pollutant under VLI, and the results obtained are shown in Fig. 6.

As shown in Fig. 6, the photolysis control in the absence of photocatalyst was found to contribute approximately 2.4 % self-degradation in 2 h under VLI. Due to this relatively small contribution, the effect of photolysis was thought to be negligible in the photocatalytic system. As seen in Fig. 6, the

$\text{Ag}_2\text{O}/\text{Ag}_3\text{VO}_4/\text{Ag}_4\text{V}_2\text{O}_7$ sample exhibited the highest photocatalytic activity compared to the other photocatalysts tested, exhibiting 99% RhB decomposition in 2 h, while the Ag_3VO_4 , $\text{Ag}_4\text{V}_2\text{O}_7$ and P25 TiO_2 affected 78%, 83% and 59% degradations in the same time period, respectively. The improved photocatalytic performance of the $\text{Ag}_2\text{O}/\text{Ag}_3\text{VO}_4/\text{Ag}_4\text{V}_2\text{O}_7$ compared to the other photocatalysts was thought to be attributed to the effects of the multi-phase $\text{Ag}_2\text{O}/\text{Ag}_3\text{VO}_4/\text{Ag}_4\text{V}_2\text{O}_7$ photocatalyst.

3.6.2. RhB degradation mechanism

To further investigate the mechanism of RhB photocatalytic degradation in the presence of $\text{Ag}_2\text{O}/\text{Ag}_3\text{VO}_4/\text{Ag}_4\text{V}_2\text{O}_7$, the changes to the UV-visible spectra of the dye during the photocatalytic reaction were investigated, and the results are shown in Fig. 7.

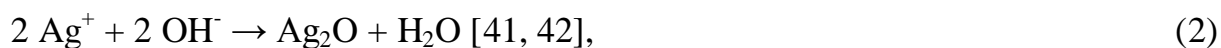
As seen in Fig. 7, the intensity of the characteristic absorption peak at 554 nm reduced significantly along the course of reaction, with progressive shifts of the absorption bands towards the blue region from 554 nm to 520 nm, in agreement with the results reported in literature on the photocatalytic degradation of RhB over TiO_2 and Bi_2WO_6 under visible light, respectively [39, 40]. Competitive reactions between the cleavage of the RhB chromophore ring structure and N-de-ethylation were thought to occur during the entire photocatalytic degradation process for

RhB. From Fig. 7, the decline at the maximum absorption wavelength of 554 nm was indicative of the cleavage of the whole conjugated chromophore structure of RhB, while the minor shifts from 554 nm to 520 nm were indicative of the stepwise N-de-ethylation of RhB. Of these processes, the cleavage of the whole conjugated chromophore structure for RhB was thought to be predominant during the observed degradation process.

3.7. Stability of $\text{Ag}_2\text{O}/\text{Ag}_3\text{VO}_4/\text{Ag}_4\text{V}_2\text{O}_7$

3.7.1. Analyses of crystal structural changes

The multi-phase material synthesized consisted of dual-phase $\text{Ag}_3\text{VO}_4/\text{Ag}_4\text{V}_2\text{O}_7$ decorated with Ag_2O NPs at the surface, and the instability of the photocatalyst under the photocatalytic conditions was thought to induce the loss crystallinity of dual-phase $\text{Ag}_3\text{VO}_4/\text{Ag}_4\text{V}_2\text{O}_7$ and the generation of Ag^0 NPs. Some Ag^+ ions from $\text{Ag}_4\text{V}_2\text{O}_7$ were thought to first react with the adsorbed hydroxyl ions (OH^-) to give rise to Ag_2O , as shown in reaction (2):



Ag_2O were unstable with prolonged photocatalytic reaction under VLI, and some of Ag_2O could be reduced to Ag^0 NPs by receiving photogenerated electrons [38]:



With the increase of quantity of Ag^0 NPs, Ag_3VO_4 was thought to be converted to pyrovanadate ($\text{Ag}_4\text{V}_2\text{O}_7$) and some Ag_2O , under prolonged photocatalytic reaction. This is shown by the following reaction:



Accordingly, the loss of crystallinity of both Ag_3VO_4 and $\text{Ag}_4\text{V}_2\text{O}_7$ promoted the generation of Ag_2O and the increase of Ag^0 NPs, as reported by Belver et al. [17]. This process decreased the crystallinity of Ag_3VO_4 during photocatalytic reaction under VLI. Although the instability of Ag_3VO_4 facilitated the transformation of Ag^+ into Ag^0 , resulting in the photocorrosion of Ag_3VO_4 in the absence of the electron acceptors, Ag^0 NPs with the SPR served as active photocatalytic sites for accepting photogenerated electrons and transferring them to the adsorbed oxygen, where more hydroxyl radicals were generated due to photogenerated holes that reacted with absorbed H_2O , which acted to enhanced photocatalytic reaction under VLI.

Structural changes to the multi-phase $\text{Ag}_2\text{O}/\text{Ag}_3\text{VO}_4/\text{Ag}_4\text{V}_2\text{O}_7$ photocatalyst occurred during the course of photocatalytic reaction, and were studied via a number of characterization techniques and investigations. The post-use characterization results are discussed in subsequent sections.

3.7.2. Post-use XRD analysis

In order to further investigate changes to the crystal structure of the multi-phase $\text{Ag}_2\text{O}/\text{Ag}_3\text{VO}_4/\text{Ag}_4\text{V}_2\text{O}_7$ photocatalyst upon exposure in the photoreactive system, XRD analyses were performed on the recycled catalysts. The post-use patterns obtained for various samples are shown in Fig. 8.

Compared to the fresh sample shown in Fig. 1, the XRD patterns obtained from the material recovered post-use and after recycling evidenced that structural changes occurred to $\text{Ag}_2\text{O}/\text{Ag}_3\text{VO}_4/\text{Ag}_4\text{V}_2\text{O}_7$ in the photosystem. In the XRD pattern shown in Fig. 8a, after reaction with 15 mg L^{-1} RhB for 2 h, an obvious loss of crystallinity of the $\text{Ag}_4\text{V}_2\text{O}_7$ structure was observed, as evidenced in the decline of major peaks at 32.93° and 31.93° . This was thought to be due to the reported instability of $\text{Ag}_4\text{V}_2\text{O}_7$ under visible light irradiation [43]. The Ag^+ ions in $\text{Ag}_4\text{V}_2\text{O}_7$ reacted with the adsorbed OH^- ions to produce Ag_2O . In addition, some lattice Ag^+ of Ag_2O was thought to be reduced to the Ag^0 by receiving photogenerated electrons during the photocatalytic reaction [38]. This was evidenced by the Ag^0 phase discovered and the major reflections which occurred at 38.10° and 44.28° for Ag^0 in the pattern (JCPDS Card No. 01-071-4613), as shown in Fig. 8b. Also, the produced Ag_2O phase was not stable in the presence of ethanol, and could be dissolved in ethanol after photocatalytic reaction according to the literature reported by Singh et al. [44] and Mehta et al. [45] due to the solubility of

this phase in the solvent. As such, the used photocatalyst was rinsed with ethanol after recovery from the degraded RhB supernatant, and then recovered from the ethanol extract by centrifugation. By comparison of the rinsed photocatalyst and the unwashed photocatalyst after use, respectively, crystallinity changes and the characteristics of these post-use photocatalysts were observed. The loss of crystallinity of $\text{Ag}_4\text{V}_2\text{O}_7$ during photocatalysis was appreciable, as observed in Fig. 8a.

The XRD pattern shown in Fig. 8b represented that of the unwashed photocatalyst after a single use in the photosystem with 15 mg L^{-1} RhB solution under VLI for 2 h. Comparison of Fig. 8b with Fig. 8a illustrates an obvious increase in the intensity of the diffraction peak for Ag^0 in the unwashed sample at 38.10° ; and was thought to be due to more $\text{Ag}_4\text{V}_2\text{O}_7$ being photocorroded, so that more Ag^+ ions from $\text{Ag}_4\text{V}_2\text{O}_7$ were reduced to Ag^0 eventually with prolonged reaction under VLI. Furthermore, the intensity of the diffraction peaks of $\text{Ag}_4\text{V}_2\text{O}_7$ at 31.93° and 32.93° were much higher than the characteristic peaks for $\text{Ag}_4\text{V}_2\text{O}_7$ shown in Fig. 8a. This was ascribed to the instability of Ag_3VO_4 with prolonged photocatalytic reaction in the presence of generated Ag^0 NPs, resulting in the conversion from Ag_3VO_4 to pyrovanadate ($\text{Ag}_4\text{V}_2\text{O}_7$), and a new generation of Ag_2O [17].

The XRD patterns of Fig. 8b and Fig. 8c were used to further investigate these structural changes in the multi-phase $\text{Ag}_2\text{O}/\text{Ag}_3\text{VO}_4/\text{Ag}_4\text{V}_2\text{O}_7$ upon cyclic use. As shown in Fig. 8c for the recycled photocatalyst used three times, more Ag^0 NPs were generated upon prolonged reaction, as shown in the intensity of diffraction peaks at 38.10° . In addition, the loss of crystallinity of Ag_3VO_4 was more severe than the sample shown in Fig. 8b, suggesting that Ag^+ ions in Ag_3VO_4 were both reduced to Ag^0 NPs and gave rise to the increase of $\text{Ag}_4\text{V}_2\text{O}_7$ phase, respectively.

3.7.3. Post-use SEM analysis

The morphologies of the synthesized multi-phase $\text{Ag}_2\text{O}/\text{Ag}_3\text{VO}_4/\text{Ag}_4\text{V}_2\text{O}_7$ photocatalysts after photocatalytic reactions were explored by SEM, in order to investigate the microstructure and morphology changes that occurred, and the images obtained are shown in Fig. 9.

No difference in morphologies was observed between Fig. 3a and Fig. 9a, indicating that the photocatalytic reaction towards dye degradation did not strongly impact the morphology of the catalyst. Comparison of Figs. 9a, 9b and 9c indicated that multi-morphology of the synthesized photocatalysts emerged after use in the photocatalytic reaction, where more Ag^0 NPs were generated during the course of VLI, as confirmed by the XRD results obtained. In addition, a new generation of two-dimensional Ag_2O nanotubes (NTs) (width: $0.2\ \mu\text{m}$ - $0.4\ \mu\text{m}$; length: $4\ \mu\text{m}$ - 40

μm) was also observed in the unwashed samples (Figs. 9b and 9c), which was mainly attributed to the loss of crystallinity of Ag_3VO_4 and $\text{Ag}_4\text{V}_2\text{O}_7$ under prolonged photocatalytic conditions [17]. As seen in Figs. 9b and 9c, two-dimensional NTs were observed and were thought to be Ag_2O , based upon the results obtained by XRD. These Ag_2O NTs were not observed in the pure rinsed sample shown in Fig. 9a, suggesting that the new generation of Ag_2O NTs resulted from both Ag_3VO_4 and $\text{Ag}_4\text{V}_2\text{O}_7$ after photocatalytic performance.

As shown in Fig. 9c, more Ag^0 NPs were obtained in the unwashed recycled sample after three runs, while the amount of Ag_2O NTs decreased. This may indicate that the loss crystallinity of both Ag_3VO_4 and $\text{Ag}_4\text{V}_2\text{O}_7$ was severe after prolonged photocatalytic reaction, resulting in the generation of more Ag_2O NTs, while Ag_2O was unstable in the reducing ambient RhB solution under VLI, and gave rise to Ag^0 NPs [44], increasing the amount of Ag^0 NPs decorated on the multi-phase photocatalyst, in good agreement with the results from XRD.

3.7.4. Post-use XPS analysis

To investigate the changes of chemical and electronic states present in the multi-phase photocatalyst, XPS analyses of the post-use $\text{Ag}_2\text{O}/\text{Ag}_3\text{VO}_4/\text{Ag}_4\text{V}_2\text{O}_7$ were discussed, and the corresponding high resolution XPS spectral patterns are shown in Figs. 10a, 10b and 10c, for Ag 3d, V 2p and O 1s states, respectively.

Comparing Ag 3d spectra in Fig. 4 and Fig. 10, the observed Ag 3d spectra of post-use sample changed markedly. The deconvolution of the Ag 3d was performed, and Ag 3d_{5/2} and Ag 3d_{3/2} spectra assigned to three sets of individual peaks centered at 367.0 eV & 373.0 eV, 367.9 eV & 373.6 eV, and 369.2 eV & 374.7 eV (dashed lines in Fig. 10a) were obtained. Of these six peaks, the peaks at 367.0 eV & 373.0 eV and 367.9 eV & 373.6 eV were ascribed to the binding energies of Ag, corresponding to Ag⁺, and peaks at 369.2 eV & 374.7 eV were ascribed to the binding energies of Ag, corresponding to Ag⁰ [30, 32, 46]. The chemical and electronic states of silver were thought to be changed during photocatalytic reactions under VLI, indicating that some Ag⁺ species were reduced into metallic silver. V 2p_{3/2} and V 2p_{1/2} spectra were observed to be broad in Fig. 10b, and were deconvoluted into two pairs of individual peaks centered at 516.0 eV & 522.6 eV, and 516.9 eV & 523.8 eV (dashed lines in Fig. 10b), corresponding to V⁵⁺, and corresponding well with the data from KVO₃ [34]. Photocatalytic reactions also influenced the chemical and electronic states of oxygen shown in Fig.10. O 1s spectra observed were changed noticeably, and deconvoluted into four separated peaks (dashed lines in Fig. 10c), centered at 529.3 eV, 530.8 eV, 531.8 eV and 533.1 eV, respectively. Of these four peaks, peaks at 529.3eV, 530.8 eV and 531.8 eV were attributed to the lattice oxygen in the heterogeneous multi-phase

photocatalysts, while the observed peak of O1s at 533.1 eV was ascribed to the adsorbed oxygen according to the literature [35].

3.7.5. Post-use optical properties

As shown in Fig. 11, the UV-Vis diffuse reflectance spectra of post-use $\text{Ag}_2\text{O}/\text{Ag}_3\text{VO}_4/\text{Ag}_4\text{V}_2\text{O}_7$ samples also revealed intrinsic absorption in the visible light region.

Compared to the fresh catalyst shown in Fig. 5, no apparent absorption peaks of two spectra shown in Figs. 11a and 11b were observed at longer wavelengths, indicating that Ag^0 NPs were present in low quantities after a single use. However, as shown in Fig. 11c, a noticeable broad peak at around 573 nm occurred in the absorption spectrum for the recycled sample used three times, and was thought to be due to the increased number of Ag^0 NPs present in the catalyst [47]. The broadening of the absorption peak was mainly due to the non-uniformity of the Ag^0 nanoparticle sizes and shapes [48]. These Ag^0 NPs both acted to increase the range of visible light absorption and to decrease the rate of recombination of e^-h^+ pairs [49] resulting in enhancing the efficiency of photogenerated e^-h^+ pairs capture by the adsorbed organic pollutants.

3.8. Role of reactive species testing

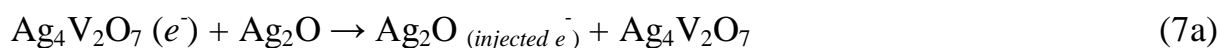
To further investigate the role of the reactive species impacting the photocatalytic degradation, quenching tests were applied to the degradation studies. Photocatalytic degradation of organic pollutants is caused by reaction with reactive species such as h^+ , e^- , $\bullet OH$ and $O_2\bullet^-$, which are generated on the surface of photocatalysts after irradiation [50]. Quenching tests for photocatalytic degradation of RhB by $Ag_2O/Ag_3VO_4/Ag_4V_2O_7$ were performed by employing various radical species scavengers, and the results are shown in Fig. 12.

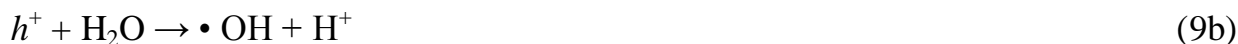
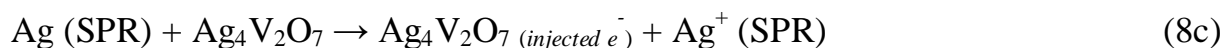
As shown in Fig. 12, without scavengers, the photocatalytic degradation of RhB was 99% within 2 h. 3 mL TBA was added to the photocatalytic reaction system as the scavenger of $\bullet OH$ [6], resulting in a reduction in the degradation of RhB to 93% at the end of the 2 h reaction. 0.015 g BQ was used as a scavenger of $O_2\bullet^-$ [51, 52], limiting the capture of photogenerated electrons by molecular oxygen (O_2) to generate $O_2\bullet^-$, and causing the photodegradation of RhB on $Ag_2O/Ag_3VO_4/Ag_4V_2O_7$ to reduce to 80%. These results indicated that the photocatalytic reaction was less likely to be restricted by reducing the amount of $\bullet OH$ and $O_2\bullet^-$. In contrast, by adding 0.15 g AO into the photocatalytic system [53, 54], the degradation was suppressed to 38% during the course of reaction, which indicated that holes played a major role in the degradation mechanism for RhB.

Therefore, holes were thought to dominate the mechanism of photocatalytic degradation of RhB under VLI for the prepared photocatalyst.

3.9. Mechanism of photocatalytic activity

A mechanism for RhB photodegradation in the presence of $\text{Ag}_2\text{O}/\text{Ag}_3\text{VO}_4/\text{Ag}_4\text{V}_2\text{O}_7$ under VLI was proposed, and the applicable reactions are given as follows:





[40, 50]

In accordance with reactions (5)-(11) and Fig. 13, the photocatalyst prepared consisted of multi-phase $\text{Ag}_2\text{O}/\text{Ag}_3\text{VO}_4/\text{Ag}_4\text{V}_2\text{O}_7$, namely $\text{Ag}_3\text{VO}_4/\text{Ag}_4\text{V}_2\text{O}_7$ decorated with Ag_2O NPs. As seen from Fig. 13, photocatalytic reaction was initiated by the absorption of photons from the visible light range with energy higher than the band gap energies of for Ag_2O , Ag_3VO_4 and $\text{Ag}_4\text{V}_2\text{O}_7$, causing the photogenerated e^-h^+ pairs to occur in the photoexcited semiconductors, in accordance with reactions (5a-5c). In addition, reaction (6) showed that these e^-h^+

pairs could either separate and move freely on the surface of photocatalysts, or recombine as energy emission under the internal electric field caused by the heterostructure, which occurred when the migration of e^-h^+ pairs was slow from the bulk to reaction sites at surface [1].

After the photoexcitation on the heterogenous photocatalyst, the photogenerated electrons were promoted to the conduction band (CB) and the holes were left at the valence band (VB) of the photocatalyst, respectively. These electrons were transferred from the CB of $Ag_4V_2O_7$ to the CB of Ag_2O firstly (reaction 7a), meanwhile, some photogenerated electrons were shifted from the CB of Ag_3VO_4 to the CB of Ag_2O as well, due to the internal electric field (reaction 7b), because CB potential of $Ag_4V_2O_7$ (-2.03 eV vs. NHE) [6] and CB potential of Ag_3VO_4 (-0.1 eV vs. NHE) [37] were more negative than that of Ag_2O (-0.04 eV vs. NHE) [38]. In addition, the CB of $Ag_4V_2O_7$ was more negative than the standard redox potential of $O_2/O_2^{\bullet-}$ (-0.33 eV vs. NHE). Therefore, electrons were able to reduce the adsorbed O_2 to $O_2^{\bullet-}$ species (reaction 9a). However, an excess of electrons accumulated in the CB of Ag_2O rather than being captured by the adsorbed O_2 molecules due to the more positive CB potential of Ag_2O than that of $O_2/O_2^{\bullet-}$ (-0.33 eV vs. NHE). The extra photogenerated electrons transferred to CB of Ag_2O could reduce Ag^+ to Ag^0 (reaction 8a), Ag^0 NPs exhibited SPR in the visible region, exciting e^-h^+ pairs on their surface. During the reaction processes,

Ag^0 NPs exhibited higher absorption intensities in the visible region ($\lambda > 410$ nm) by absorbing photons, in which, one Ag^0 nanoparticle could absorb one visible light photon resulting in the effectively polarized state by plasmon resonance of silver, causing effective separation of the SPR-excited electrons and holes [55] (reaction 8b). And these electrons were transferred from the SPR-excited Ag^0 NPs to CB of $\text{Ag}_4\text{V}_2\text{O}_7$ [56] (reaction 8c), while, holes caused more $\bullet\text{OH}$ by reacted with absorbed H_2O (reaction 9b). Therefore, more electrons transferred happened from the CB of $\text{Ag}_4\text{V}_2\text{O}_7$ to that of Ag_2O (reaction 7a) due to the plasmon resonance of silver.

Holes also migrated from the VB of Ag_3VO_4 to VB of Ag_2O then to VB of $\text{Ag}_4\text{V}_2\text{O}_7$ because of the internal electric field present, as shown in reactions (7c and 7d), accompanied with more positive VB potential, Ag_3VO_4 preferentially oxidized OH^- to give $\bullet\text{OH}$ ($\bullet\text{OH}/\text{OH}^-$, 1.55 eV vs. NHE) (reaction 9b), H_2O to give O_2 ($\text{O}_2/\text{H}_2\text{O}$, 1.23 eV vs. NHE) (reaction 9c), and OH^- to give O_2 (O_2/OH^- , 0.4 eV vs. NHE) (reaction 9d) [57]. Ag_2O was able to give rise to reactions 9c and 9d as well, due to the internal electric field present. In addition, holes transferred to VB of $\text{Ag}_4\text{V}_2\text{O}_7$ were trapped by OH^- ions originating from hydrolysis of H_2O at surface to yield O_2 and protons (H^+) (reaction 9d). Furthermore, the generated $\text{O}_2\bullet^-$ radicals at CB of $\text{Ag}_4\text{V}_2\text{O}_7$ combined with the generated protons to yield $\text{HO}_2\bullet$ radicals (reaction 10a). Finally, additional $\bullet\text{OH}$ radicals were generated via $\text{HO}_2\bullet$

radicals reacting with both photoexcited electrons and protons (reaction 10b) [58]. During the whole photocatalytic degradation, photogenerated holes played a significant role of generating the strong oxidant $\bullet\text{OH}$ radicals, resulting in the direct oxidization of RhB (reactions 11a and 11b) [56] on the surface of $\text{Ag}_2\text{O}/\text{Ag}_3\text{VO}_4/\text{Ag}_4\text{V}_2\text{O}_7$. Therefore, this high photocatalytic performance was attributed to the positive effects between the photocatalysis of multi-phase $\text{Ag}_2\text{O}/\text{Ag}_3\text{VO}_4/\text{Ag}_4\text{V}_2\text{O}_7$ and SPR of Ag^0 NPs [56].

4. Conclusions

Multi-phase $\text{Ag}_2\text{O}/\text{Ag}_3\text{VO}_4/\text{Ag}_4\text{V}_2\text{O}_7$ photocatalyst was prepared through a facile hydrothermal method. Characterization tests indicated that dual-phase Ag_3VO_4 and $\text{Ag}_4\text{V}_2\text{O}_7$ were present in the system and were surface-decorated by Ag_2O NPs. Although each single phase (Ag_2O , $\text{Ag}_4\text{V}_2\text{O}_7$ and Ag_3VO_4), suffered from structural changes and loss of crystallinity in the photocatalytic system, the existence of the produced Ag^0 NPs induced positive effects of SPR on photocatalysis, which promoted an overall high photocatalytic performance towards the degradation of RhB under VLI. A new generation of Ag_2O nanotube-like structures and the increase of Ag^0 formed from the morphological changes that occurred under the photocatalytic reaction were observed. A mechanism was proposed for the photocatalytic degradation of RhB.

Acknowledgments

This work was funded by the Natural Sciences and Engineering Research Council of Canada (NSERC). The authors would like to thank Dr. Alexander Mommers at the Center for Catalysis Research and Innovation, and the Department of Earth Sciences at the University of Ottawa, as well as Dr. Jianqun Wang at Carleton University for help with sample characterizations. The Chinese Scholarship Council is also acknowledged for financial support.

References

- [1] A. Kudo, Y. Miseki, *Chem. Soc. Rev.* 38 (2009) 253-278.
- [2] A. Walsh, Y. Yan, M.N. Huda, M.M. Al-Jassim, S.-H. Wei, *Chem. Mater.* 21 (2009) 547-551.
- [3] D.Y. Shahriari, N. Erdman, U.T.M. Haug, M.C. Zarzyczny, L.D. Marks, K.R. Poeppelmeier, *J. Phys. Chem. Solids* 64 (2003) 1437-1441.
- [4] C. Linke, M. Jansen, *Inorg. Chem.* 33 (1994) 2614-2616.
- [5] X. Hu, C. Hu, *J. Solid State Chem.* 180 (2007) 725-732.
- [6] J. Wang, X. Yang, J. Chen, J. Xian, S. Meng, Y. Zheng, Y. Shao, D. Li, *J. Am. Ceram. Soc.* 97 (2014) 267-274.

- [7] S. Zhang, W. Li, C. Li, J. Chen, *J. Phys. Chem. B* 110 (2006) 24855-24863.
- [8] H. Kato, H. Kobayashi, A. Kudo, *J. Phys. Chem. B* 106 (2002) 12441-12447.
- [9] Y. Maruyama, H. Irie, K. Hashimoto, *J. Phys. Chem. B* 110 (2006) 23274-23278.
- [10] S. Ouyang, N. Kikugawa, D. Chen, Z. Zou, J. Ye, *J. Phys. Chem. C* 113 (2009) 1560-1566.
- [11] G. Dai, J. Yu, G. Liu, *J. Phys. Chem. C* 116 (2012) 15519-15524.
- [12] Y. Bi, H. Hu, S. Ouyang, G. Lu, J. Cao, J. Ye, *Chem. Commun.* 48 (2012) 3748-3750.
- [13] A. Kubacka, M. Fernández-García, G. Colón, *Chem. Rev.* 112 (2011) 1555-1614.
- [14] R. Konta, H. Kato, H. Kobayashi, A. Kudo, *Phys. Chem. Chem. Phys.* 5 (2003) 3061-3065.
- [15] X. Tao, Q. Hong, T. Xu, F. Liao, *J. Mater. Sci. - Mater. Electron.* 25 (2014) 3480-3485.
- [16] C. Dong, K.-L. Wu, X.-W. Wei, X.-Z. Li, L. Liu, T.-H. Ding, J. Wang, Y. Ye, *CrystEngComm* 16 (2014) 730-736.

- [17] C. Belver, C. Adán, S. García-Rodríguez, M. Fernández-García, *Chem. Eng. J.* 224 (2013) 24-31.
- [18] Q. Xiang, J. Yu, B. Cheng, H.C. Ong, *Chem. Asian J.* 5 (2010) 1466-1474.
- [19] B. Neppolian, H.C. Choi, S. Sakthivel, B. Arabindoo, V. Murugesan, *J. Hazard. Mater.* 89 (2002) 303-317.
- [20] D. Peng, Z. Min, X. Zhonglei, C. Lihong, *J. Nanomater.* 2015 (2015) 7.
- [21] J. Xue, S. Ma, Y. Zhou, Z. Zhang, X. Wu, C. She, *RSC Adv.* 5 (2015) 3122-3129.
- [22] P.Q. Wang, Y. Bai, P.Y. Luo, J.Y. Liu, *Micro Nano Lett.* 8 (2013) 340-344.
- [23] L. Xu, B. Wei, W. Liu, H. Zhang, C. Su, J. Che, *Nanoscale Res. Lett.* 8 (2013) 1-16.
- [24] W. Zhou, H. Liu, J. Wang, D. Liu, G. Du, J. Cui, *ACS Appl. Mater. Interfaces* 2 (2010) 2385-2392.
- [25] C.-M. Huang, G.-T. Pan, Y.-C.M. Li, M.-H. Li, T.C.K. Yang, *Appl. Catal., A* 358 (2009) 164-172.
- [26] C.-M. Huang, K.-W. Cheng, G.-T. Pan, W.-S. Chang, T.C.K. Yang, *Chem. Eng. Sci.* 65 (2010) 148-152.

- [27] D. Yang, H. Liu, L. Liu, S. Sarina, Z. Zheng, H. Zhu, *Nanoscale* 5 (2013) 11011-11018.
- [28] G.-T. Pan, M.-H. Lai, R.-C. Juang, T.-W. Chung, T.C.K. Yang, *Ind. Eng. Chem. Res.* 50 (2011) 2807-2814.
- [29] K.S. Raju, M.K. Pour Seydei, S.A. Suthanthiraraj, *Mater. Lett.* 19 (1994) 65-68.
- [30] W.-S. Wang, H. Du, R.-X. Wang, T. Wen, A.-W. Xu, *Nanoscale* 5 (2013) 3315-3321.
- [31] H.S. Shin, H.C. Choi, Y. Jung, S.B. Kim, H.J. Song, H.J. Shin, *Chem. Phys. Lett.* 383 (2004) 418-422.
- [32] M.S.A.S. Shah, M. Nag, T. Kalagara, S. Singh, S.V. Manorama, *Chem. Mater.* 20 (2008) 2455-2460.
- [33] W. Liu, Y. Yu, L. Cao, G. Su, X. Liu, L. Zhang, Y. Wang, *J. Hazard. Mater.* 181 (2010) 1102-1108.
- [34] D. Courcot, A. Ponchel, B. Grzybowska, Y. Barbaux, M. Rigole, M. Guelton, J.P. Bonnelle, *Catal. Today* 33 (1997) 109-118.
- [35] Z. Sun, J. Guo, S. Zhu, L. Mao, J. Ma, D. Zhang, *Nanoscale* 6 (2014) 2186-2193.

- [36] H.H. Huang, X.P. Ni, G.L. Loy, C.H. Chew, K.L. Tan, F.C. Loh, J.F. Deng, G.Q. Xu, *Langmuir* 12 (1996) 909-912.
- [37] G. Trimarchi, H. Peng, J. Im, A.J. Freeman, V. Cloet, A. Raw, K.R. Poepelmeier, K. Biswas, S. Lany, A. Zunger, *Phys. Rev. B: Condens. Matter* 84 (2011).
- [38] W. Jiang, X. Wang, Z. Wu, X. Yue, S. Yuan, H. Lu, B. Liang, *Ind. Eng. Chem. Res.* 54 (2015) 832-841.
- [39] Z. He, C. Sun, S. Yang, Y. Ding, H. He, Z. Wang, *J. Hazard. Mater.* 162 (2009) 1477-1486.
- [40] T. Wu, G. Liu, J. Zhao, H. Hidaka, N. Serpone, *J. Phys. Chem. B* 102 (1998) 5845-5851.
- [41] F.A.W. Cotton, Geoffrey, New York: Interscience. (1966) 1042.
- [42] G. Wang, X. Ma, B. Huang, H. Cheng, Z. Wang, J. Zhan, X. Qin, X. Zhang, Y. Dai, *J. Mater. Chem.* 22 (2012) 21189-21194.
- [43] R. Rotival, Y. Corvis, Y. Cartigny, P. Negrier, M. Marchivie, S. Massip, I. Gana, P. Lemoine, P. Espeau, *CrystEngComm* 15 (2013) 7970-7980.
- [44] V.N. Singh, B. Rajmehta, R.K. Joshi, F.E. Kruis, *J. Nanomater.* 2007 (2007) 1-5.

- [45] B.R. Mehta, V.N. Singh, *Pramana-J. Phys* 65 (2005) 949-958.
- [46] P. Wang, B. Huang, Z. Lou, X. Zhang, X. Qin, Y. Dai, Z. Zheng, X. Wang, *Chem. Eur. J.* 16 (2010) 538-544.
- [47] G. Li, K.H. Wong, X. Zhang, C. Hu, J.C. Yu, R.C.Y. Chan, P.K. Wong, *Chemosphere* 76 (2009) 1185-1191.
- [48] X. Zhang, Y.L. Chen, R.-S. Liu, D.P. Tsai, *Rep. Prog. Phys.* 76 (2013) 046401.
- [49] D. Zhang, F. Zeng, *Res. Chem. Intermed.* 36 (2010) 1055-1063.
- [50] J. Zhao, C. Chen, W. Ma, *Top. Catal.* 35 (2005) 269-278.
- [51] M. Styliadi, D.I. Kondarides, X.E. Verykios, *Appl. Catal., B* 47 (2004) 189-201.
- [52] P. Raja, A. Bozzi, H. Mansilla, J. Kiwi, *J. Photochem. Photobiol., A* 169 (2005) 271-278.
- [53] H. Lin, H. Ye, S. Chen, Y. Chen, *RSC Adv.* 4 (2014) 10968-10974.
- [54] W. Li, D. Li, W. Zhang, Y. Hu, Y. He, X. Fu, *J. Phys. Chem. C* 114 (2010) 2154-2159.
- [55] J. Gamage McEvoy, W. Cui, Z. Zhang, *Appl. Catal., B* 144 (2014) 702-712.

[56] Q. Zhu, W.S. Wang, L. Lin, G.Q. Gao, H.L. Guo, H. Du, A.W. Xu, J. Phys. Chem. C 117 (2013) 5894-5900.

[57] A.J. Bard, R. Parsons, J. Jordan, Marcel Dekker: New York (1985).

[58] S. Horikoshi, H. Hidaka, N. Serpone, Environ. Sci. Technol. 36 (2002) 1357-1366.

Figure captions

Fig. 1: XRD pattern of fresh multi-phase $\text{Ag}_2\text{O}/\text{Ag}_3\text{VO}_4/\text{Ag}_4\text{V}_2\text{O}_7$ photocatalyst.

Fig. 2: TEM images of (a and b) multi-phase $\text{Ag}_2\text{O}/\text{Ag}_3\text{VO}_4/\text{Ag}_4\text{V}_2\text{O}_7$; (c) high-resolution TEM of multi-phase $\text{Ag}_2\text{O}/\text{Ag}_3\text{VO}_4/\text{Ag}_4\text{V}_2\text{O}_7$ composite (SAED patterns shown inset).

Fig. 3: (a): SEM image of fresh multi-phase $\text{Ag}_2\text{O}/\text{Ag}_3\text{VO}_4/\text{Ag}_4\text{V}_2\text{O}_7$ photocatalyst and corresponding EDS data for (b).

Fig. 4: XPS spectra of (a): Ag 3d, (b): V 2p and (c): O1s.

Fig. 5: UV-Vis diffuse reflectance spectra (DRS) of various fresh samples.

Fig. 6: Photocatalytic degradation of RhB (15 mg L^{-1}) in the presence of $\text{Ag}_2\text{O}/\text{Ag}_3\text{VO}_4/\text{Ag}_4\text{V}_2\text{O}_7$, Ag_3VO_4 , $\text{Ag}_4\text{V}_2\text{O}_7$ and P25 as well as the photolysis of RhB under VLI for 2 h, respectively.

Fig. 7: UV-Visible spectra of RhB during the course of photocatalytic degradation by $\text{Ag}_2\text{O}/\text{Ag}_3\text{VO}_4/\text{Ag}_4\text{V}_2\text{O}_7$.

Fig. 8: XRD patterns of various post-use multi-phase $\text{Ag}_2\text{O}/\text{Ag}_3\text{VO}_4/\text{Ag}_4\text{V}_2\text{O}_7$ photocatalysts; **(a):** recycled sample after a single use (rinsed with ethanol after use); **(b):** recycled sample after a single use (unwashed) and **(c):** recycled sample after three uses (unwashed).

Fig. 9: SEM images of various post-use multi-phase $\text{Ag}_2\text{O}/\text{Ag}_3\text{VO}_4/\text{Ag}_4\text{V}_2\text{O}_7$ photocatalysts; **(a):** recycled sample after a single use (rinsed with ethanol after use); **(b):** recycled sample after a single use (unwashed) and **(c):** recycled sample after three uses (unwashed).

Fig. 10: XPS spectra of post-use multi-phase $\text{Ag}_2\text{O}/\text{Ag}_3\text{VO}_4/\text{Ag}_4\text{V}_2\text{O}_7$ photocatalysts; **(a):** Ag 3d, **(b):** V 2p and **(c):** O1s.

Fig. 11: UV-Vis diffuse reflectance spectra (DRS) of post-use $\text{Ag}_2\text{O}/\text{Ag}_3\text{VO}_4/\text{Ag}_4\text{V}_2\text{O}_7$ samples prepared via hydrothermal method; **(a):** recycled sample after a single use (rinsed with ethanol after use); **(b):** recycled sample after a single use (unwashed) and **(c):** recycled sample after three uses (unwashed).

Fig. 12: Quenching tests for photocatalytic degradation of RhB by $\text{Ag}_2\text{O}/\text{Ag}_3\text{VO}_4/\text{Ag}_4\text{V}_2\text{O}_7$ under different conditions with VLI.

Fig. 13: Photocatalytic mechanism of $\text{Ag}_2\text{O}/\text{Ag}_3\text{VO}_4/\text{Ag}_4\text{V}_2\text{O}_7$ over RhB under VLI.

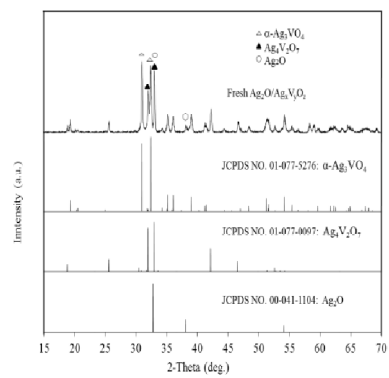


Fig. 1

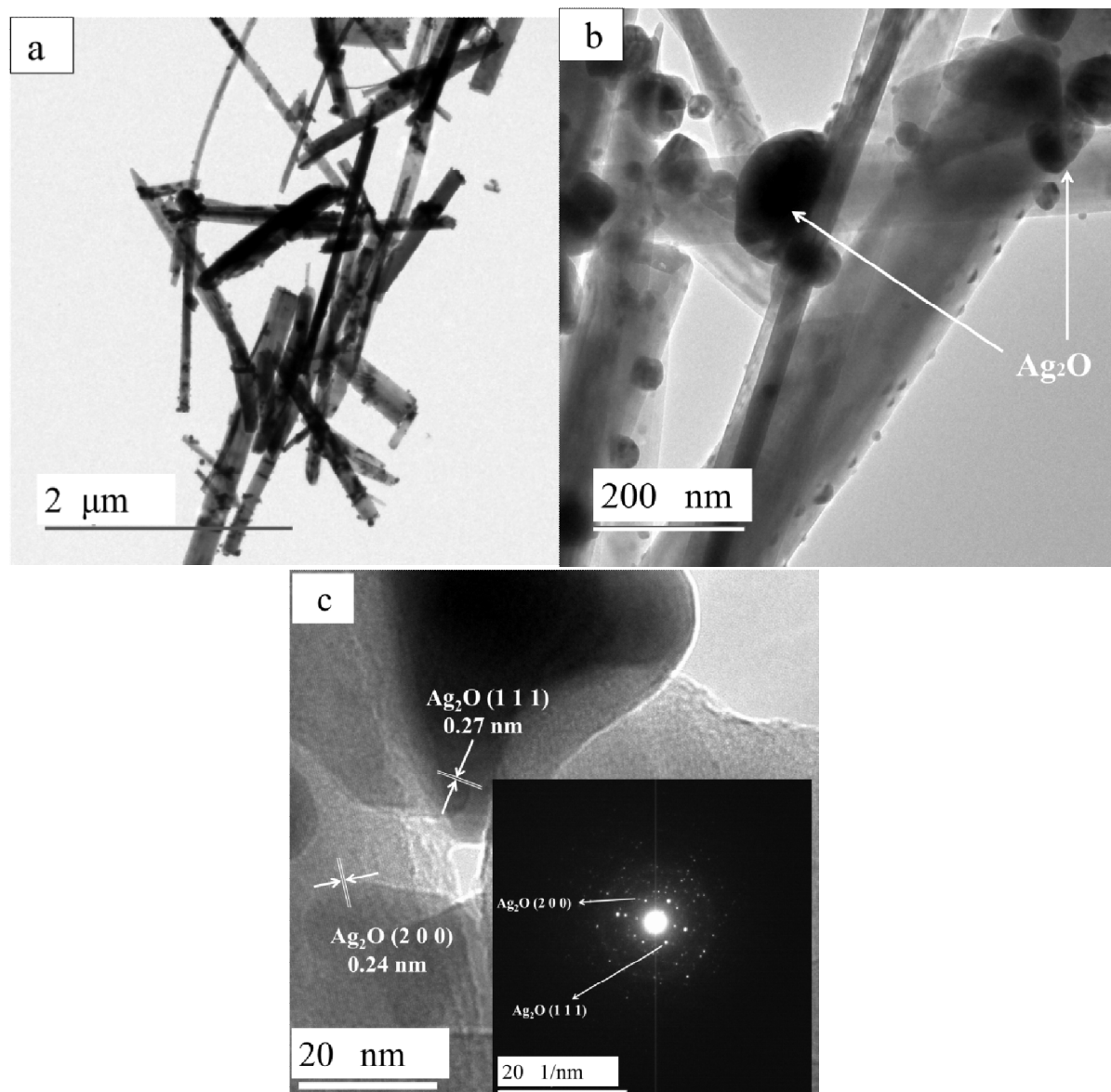


Fig. 2

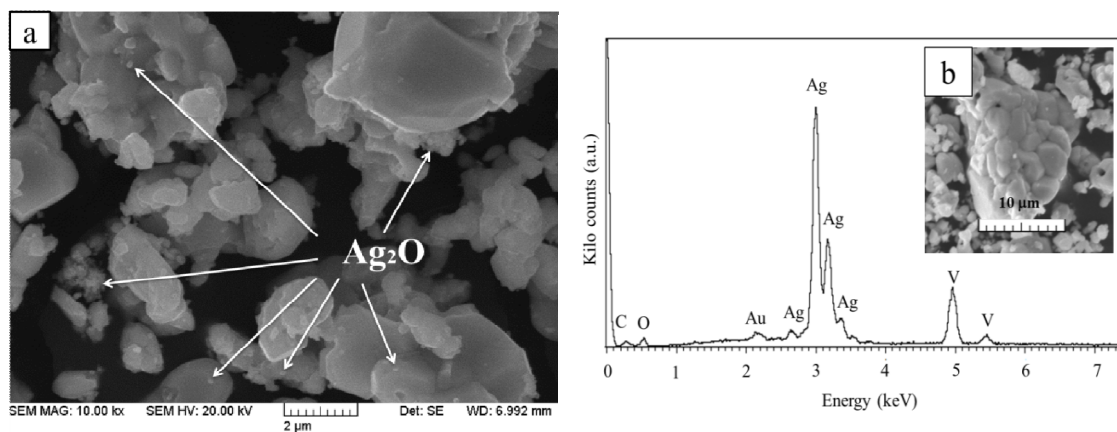


Fig. 3

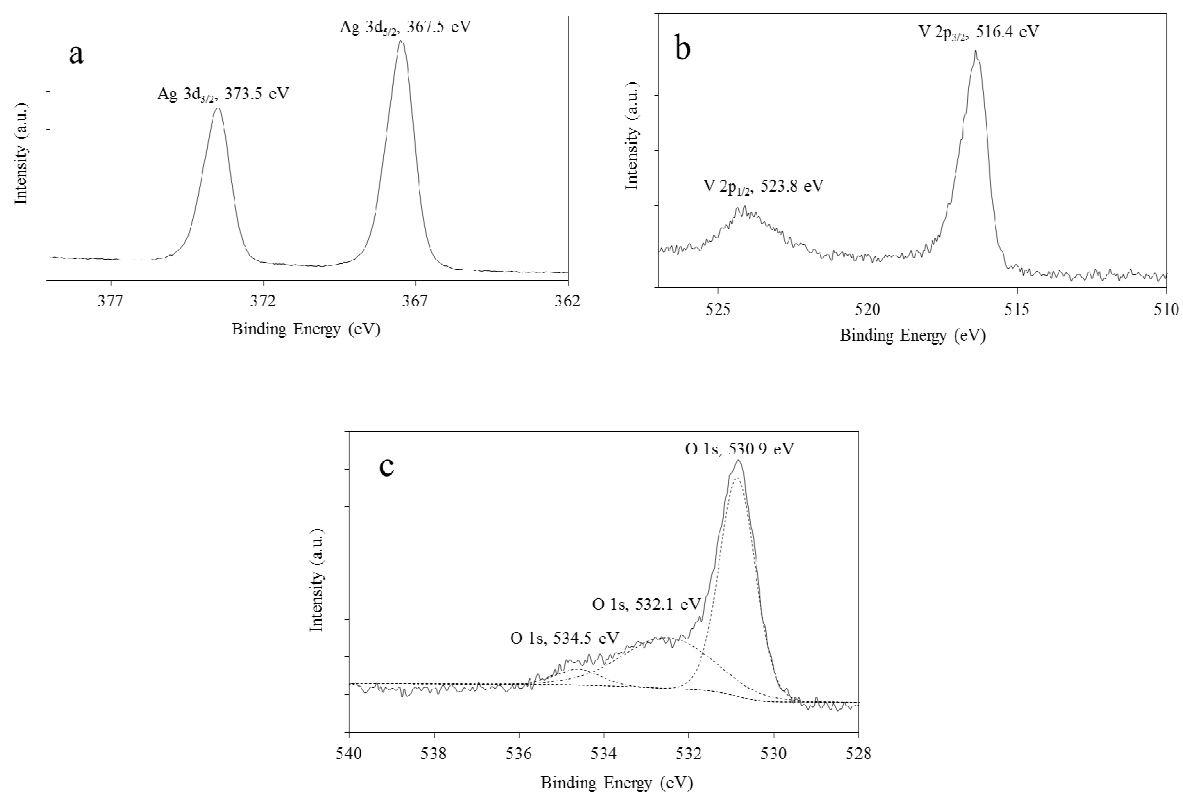


Fig. 4

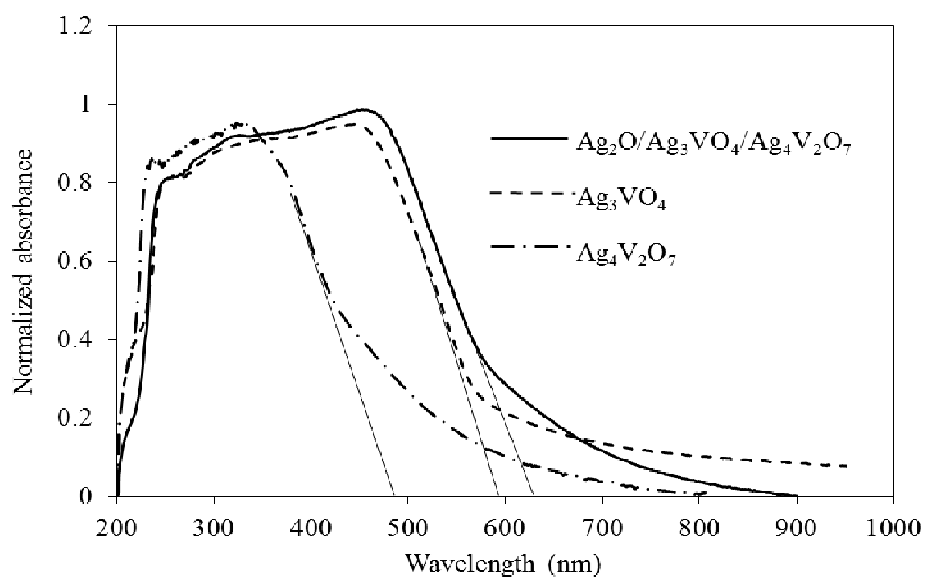


Fig. 5

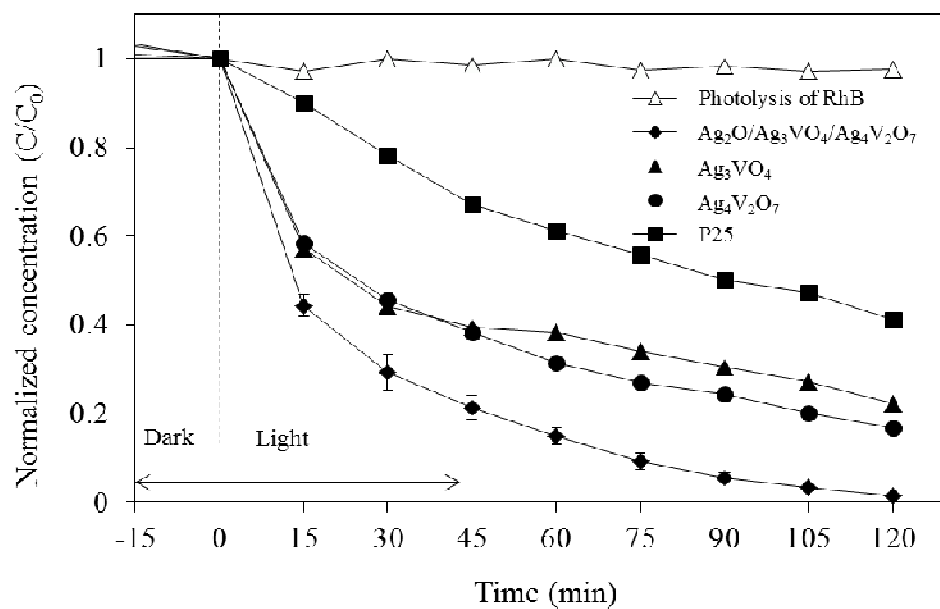


Fig. 6

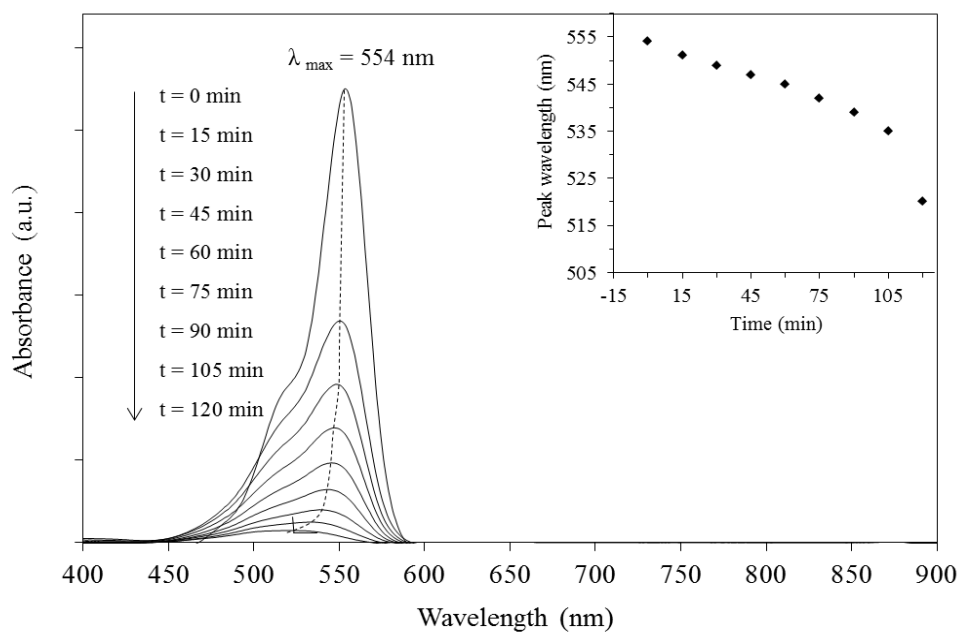


Fig. 7

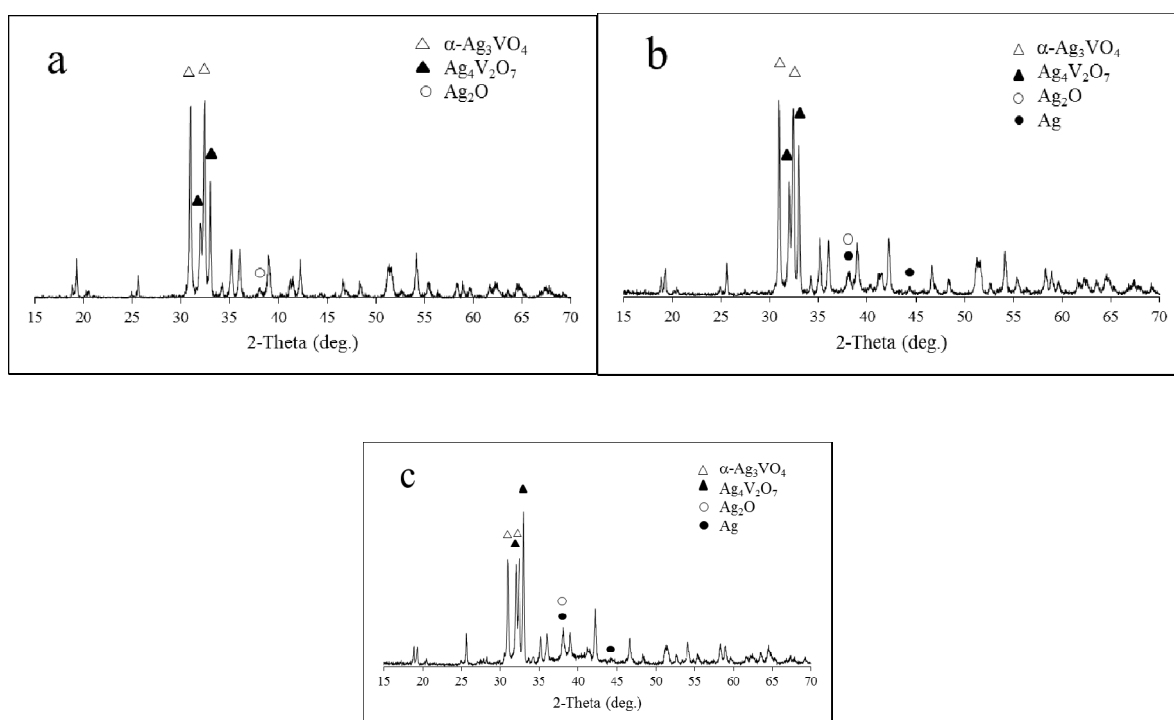
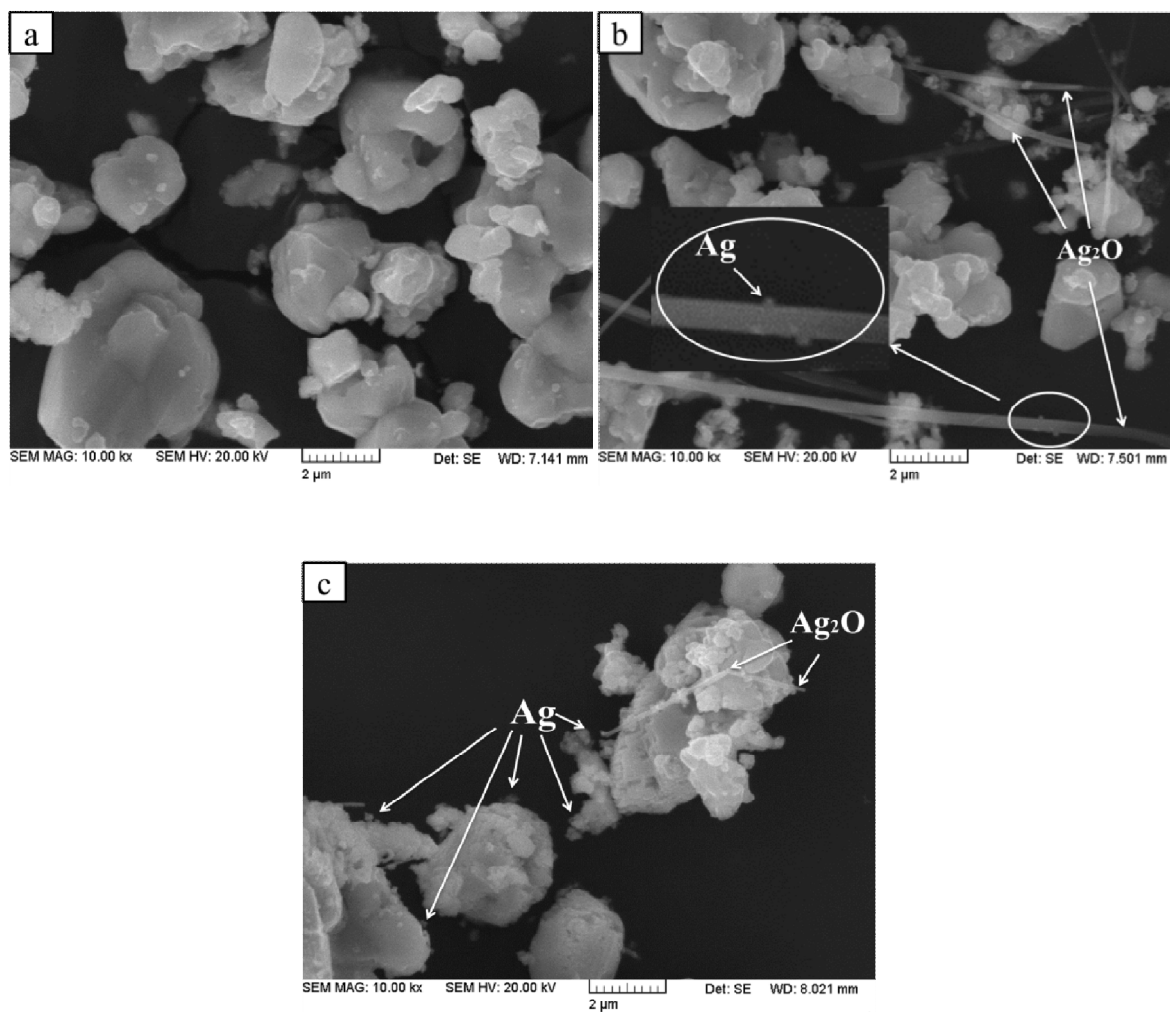
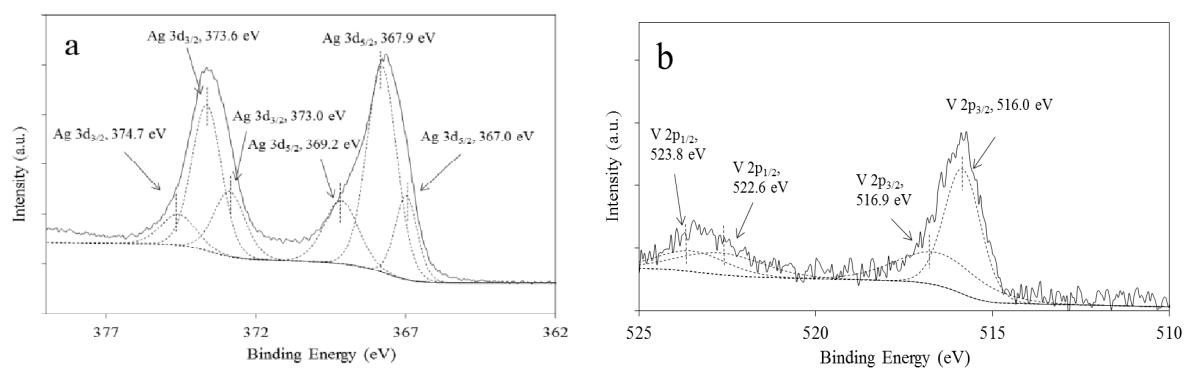
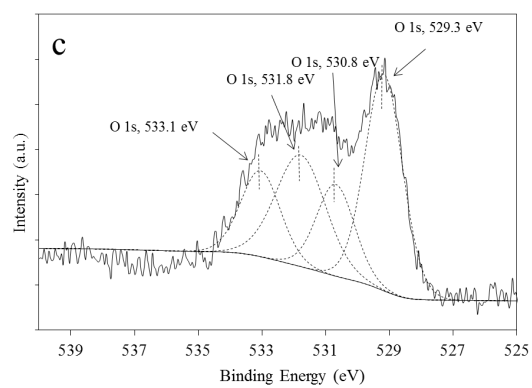
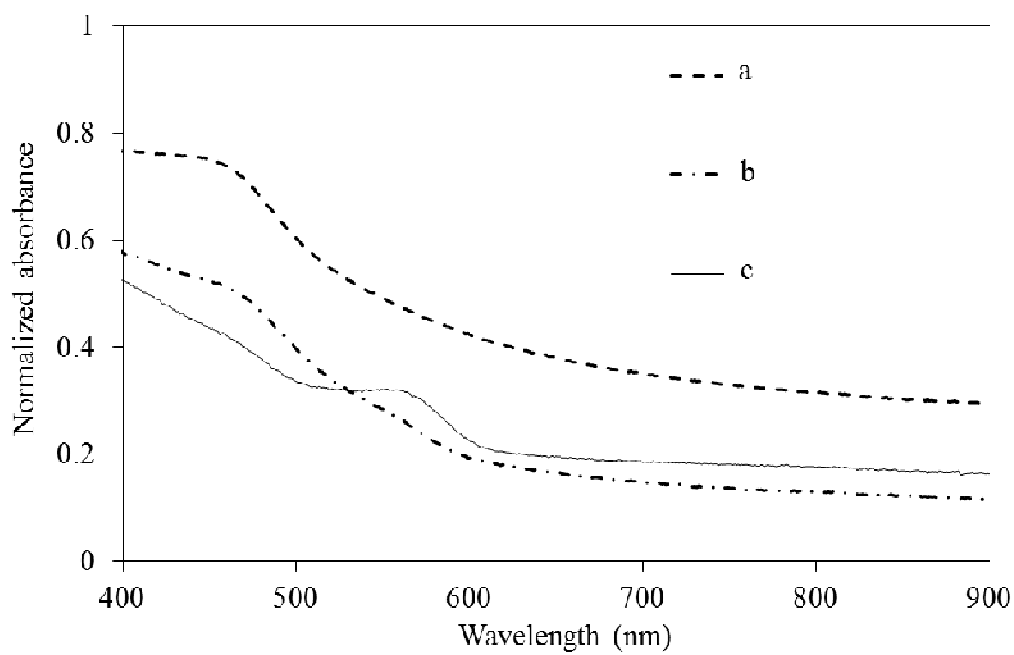
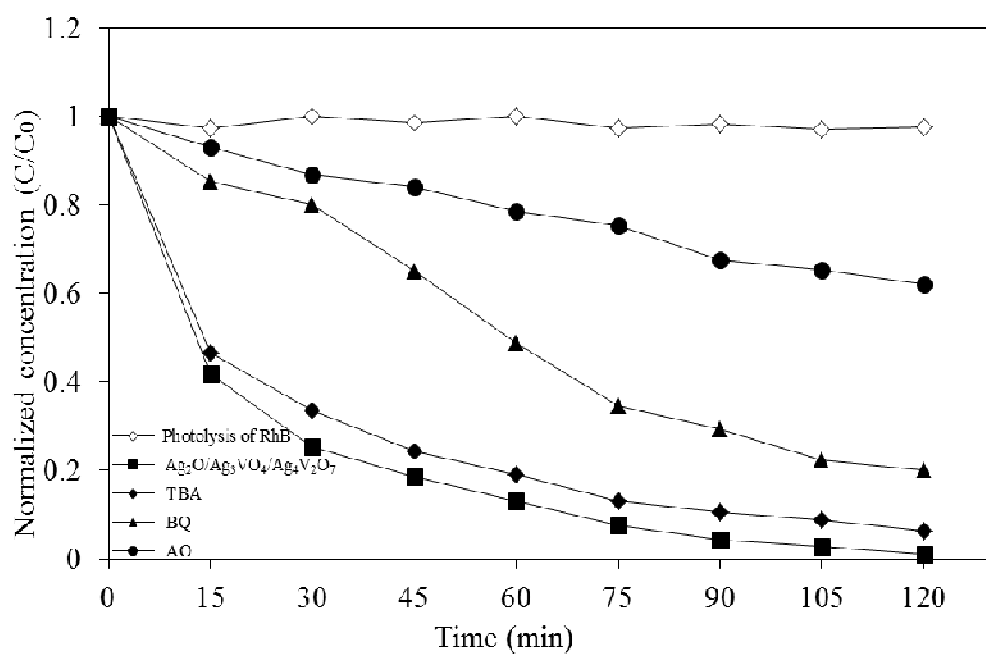


Fig. 8

**Fig. 9**

**Fig. 10****Fig. 11**

**Fig. 12**

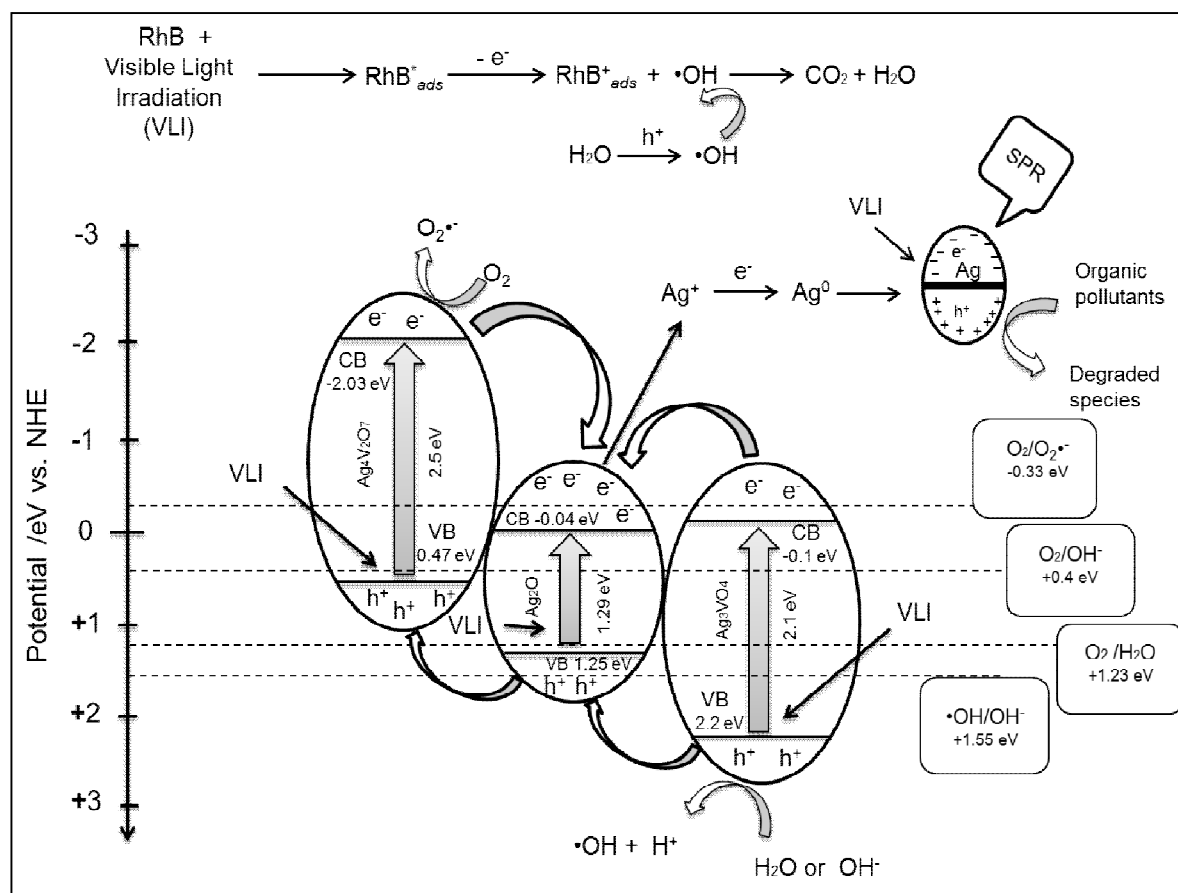


Fig. 13